# Global emergence of regional heatwave hotspots outpaces climate model projections

**K. Kornhuber[1,2,3,4*], S. Bartusek[2,5], R. Seager[2], H. J. Schellnhuber[1*], M. Ting[2,3]**

[1]International Institute for Applied Systems Analysis, Laxenburg, Austria
[2]Lamont-Doherty Earth Observatory, Columbia University, New York, NY, United States
[3]Columbia Climate School, Columbia University, New York, NY, United States
[4]Potsdam Institute for Climate Impact Research, Potsdam, Germany
[5]Department of Earth and Environmental Sciences, Columbia University, NY, United States

*Corresponding authors: kornhuber@iiasa.ac.at, schellnhuber@iiasa.ac.at

**Abstract:** Multiple recent record shattering weather events raise questions about the adequacy of climate models to effectively predict and prepare for unprecedented climate impacts on human life, infrastructure, and ecosystems. Here we show that extreme heat in several regions globally is increasing significantly and faster in magnitude than what state-of-the-art climate models have predicted under present warming even after accounting for their regional summer background warming. Across all global land area, models underestimate positive trends exceeding 0.5 °C per decade in widening of the upper tail width of extreme surface temperature distributions by a factor of 4.1 compared to reanalysis data, and exhibit a lower fraction of significantly-increasing trends overall. This highlights the need to better understand and model the drivers of extreme heat and to rapidly mitigate greenhouse gas emissions to avoid further harm from unexpected weather events.

**Significance Statement:** Heatwaves can lead to considerable impacts on societal and natural systems. An accurate simulation of their response to anthropogenic activity is important for adequate adaptation to potential climate futures. Here we quantify the behavior of extreme tails of local surface temperature distributions in reanalysis data. We find the emergence of various heatwave hotspots where the hottest 2% of the days per year are warming significantly faster than moderate heat days. We further find that output state-of-the-art climate models underestimate these trends over many regions and with a factor 4.1 bias for trends over 0.5 °C per decade. Our findings highlight the need to better understand and model extreme heat and to rapidly mitigate greenhouse gas emissions to avoid further harm.

**Keywords:** Heatwaves, Extreme Weather, Climate Change

**Classification:** Physical Sciences/Earth, Atmospheric, and Planetary Sciences

The frequency and magnitude of extreme weather events that exceeded the margins of local and regional climatology by multiple standard deviations in recent years have caused substantial impacts on ecological and social systems and attracted much attention in the public and scientific arenas. Early examples of such "record-shattering" heat events (Fischer et al., 2021) include the European and Russian heat waves of 2003, 2010, and 2018 (Barriopedro et al., 2011; Kornhuber et al., 2019; Mitchell et al., 2019; Rousi et al., 2023; Schär et al., 2004) and the Siberian heat wave of 2020 (Gloege et al., 2022; Overland & Wang, 2021). More recently the 2021 heat wave in the North American Pacific Northwest (Bartusek et al., 2022; Thompson et al., 2022; White et al., 2023) (Fig. 1a) and the sequential European heatwaves of 2022 (Fig. 1b), to which more than a seasonal total of 60.000 heat related deaths were attributed (Ballester et al., 2023), occurred in synchrony with record breaking heatwaves in North America and China. Record breaking heat returned to large parts of North America, Europe, and China in 2023 which also featured a record-breaking heatwave and severe wildfires in central Asia (Fig. 1c) (S. Perkins-Kirkpatrick et al., 2024; Zachariah et al., 2023). The observed long-term increase in extreme heat events can be attributed to anthropogenic activities, the rise of greenhouse gas concentrations in the atmosphere and their associated warming (Intergovernmental Panel on Climate Change, 2023; Robinson et al., 2021).

In the global average, this warming has been accurately predicted by different generations of climate models (Hausfather et al., 2020). The large and unexpected margins by which recent regional-scale extremes have broken earlier records, however, have raised questions about the degree to which climate models can provide adequate estimates of relations between global mean temperature changes and regional climate risks from extreme weather.

The interacting processes associated with extreme heat can cause the tails of the distributions to increase faster than the mean, with effects on regional temperature distributions (Barriopedro et al., 2023; McKinnon & Simpson, 2022). As key heatwave drivers, soil moisture deficiencies, surface air temperature and high-pressure systems constitute a tightly linked interacting trifold that can drive heat into extreme ranges. Bartusek et al. (Bartusek et al., 2022) exemplified the framework of climate-change driven non-linear interactions based on the case of the 2021 Pacific Northwest heatwave showing that extreme anomalies of common drivers can push a linear dependence structure among the three variables into a nonlinear regime. These relationships are complex and can still pose challenges to models on a regional scale. Throughout multiple generations of Coupled Model Intercomparison Projects, models have predicted that daily surface temperature variability during the warm season should increase over most land areas in response to global warming, in contrast to strongly-decreasing variability outside the warm season especially at high latitudes

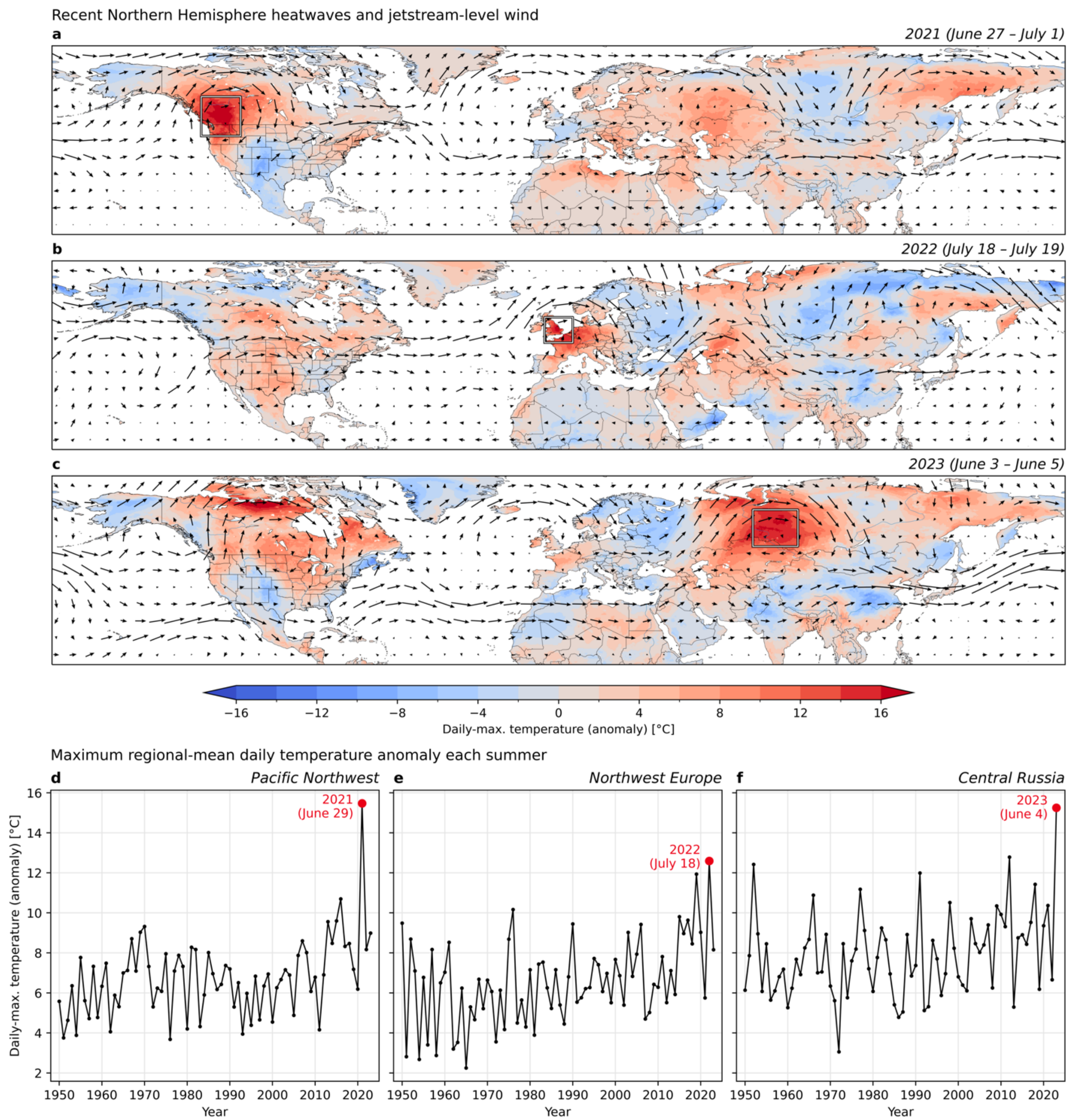


**Figure 1 Global patterns of recent record-breaking heatwaves and their temporal context.** Upper-level wind patterns (300 hPa) and 2-meter temperature anomaly fields of the Northern Hemisphere during the **a** 2021 Pacific Northwest heatwave in North America, **b** the Western European Heatwave in July 2022 and **c** the Siberian heatwave in June 2023. **d-f** Time series for the years 1950 - 2022 of the hottest daily-maximum temperature (Tx) anomaly relative to 1981 - 2010 of each summer (June – August), for the regions indicated by the boxes in **a**-**c.** The record-breaking values of regional-mean *Tx* and their dates are highlighted (red dot) in each time series.

(Donat et al., 2017; Fischer & Schär, 2010; Schär et al., 2004; Screen, 2014). However, comparing of observed trends in the far tail of extreme temperature distributions to modeled trends over the historical period remains relatively unexplored (Bathiany et al., 2018; Donat et al., 2017; Huntingford et al., 2024; McKinnon & Simpson, 2022).

Here explore we explore trends in extreme temperatures by focussing on the warming of the extreme tails compared to trends in warm-season mean for each gridpoint. The manuscript is structured as follows: we first assess trends in the extreme upper tail of local temperature distributions compared to warm-season warming over the past seven decades, to identify regional heatwave hotspots using a range of available reanalysis products (Fig. 2). We then compare the observed trends with those based on a large number of state-of-the-art model experiments from the HighResMIP project (Haarsma et al., 2016) consisting of a range of model resolutions and set-ups, fully coupled and forced with observed SSTs (Fig.3) and then discuss the local and global discrepancies (Fig. 4). We conclude with a discussion of physical mechanisms that might not be accurately captured in models and suggestions on how to move forward.

**Results**

Trends in the most extreme daily maximum near surface temperatures (Tx) values per year are greater than what is expected from a simple shift in the summer mean (i.e., 99$^{th}$ and 87.5$^{th}$ percentile values increasing by the same amounts) in several highly populated regions globally (Fig. 2a). Fig. 2a displays observed regional changes in the most extreme values (99$^{th}$ percentile) per year Tx per grid-point compared to changes in less extreme values, seasonal-scale values (87.5$^{th}$ percentile, as the average between the 75$^{th}$ and 100$^{th}$ percentile, the limits of the upper quartile) based on ERA5 reanalysis data from 1958-2022 (Hersbach et al., 2020). The most intense signal is observed in Western Europe (Fig. 2b, box b in Fig.2a), as has been reported elsewhere (Patterson, 2023; Rousi et al., 2022; Vautard et al., 2023)6/6/24 6:13:00 PM. This is a robust signal found in a series of reanalysis (JRA-55) and regionally accurate datasets (E-OBS). Our analysis reveals a set of additional regions globally in which the most extreme temperatures within a year are rising significantly faster than the warmest quarter of days (non-stippled regions in Fig. 2a, Fig. 2 b-i,). Among those are central China, southern South America, the Arabian Peninsula, Eastern Australia, Japan and Korea, and high latitude regions of Canada and Greenland. In the highest-latitude regions, JRA-55 trends are weaker, though still towards the extreme end of the modeled trend distributions. Here reanalysis products disagree on the strength of the trends, possibly due to more challenging data aggregation over these regions and the fact that JRA-55 Tx is calculated from 6-hourly instead of hourly data.

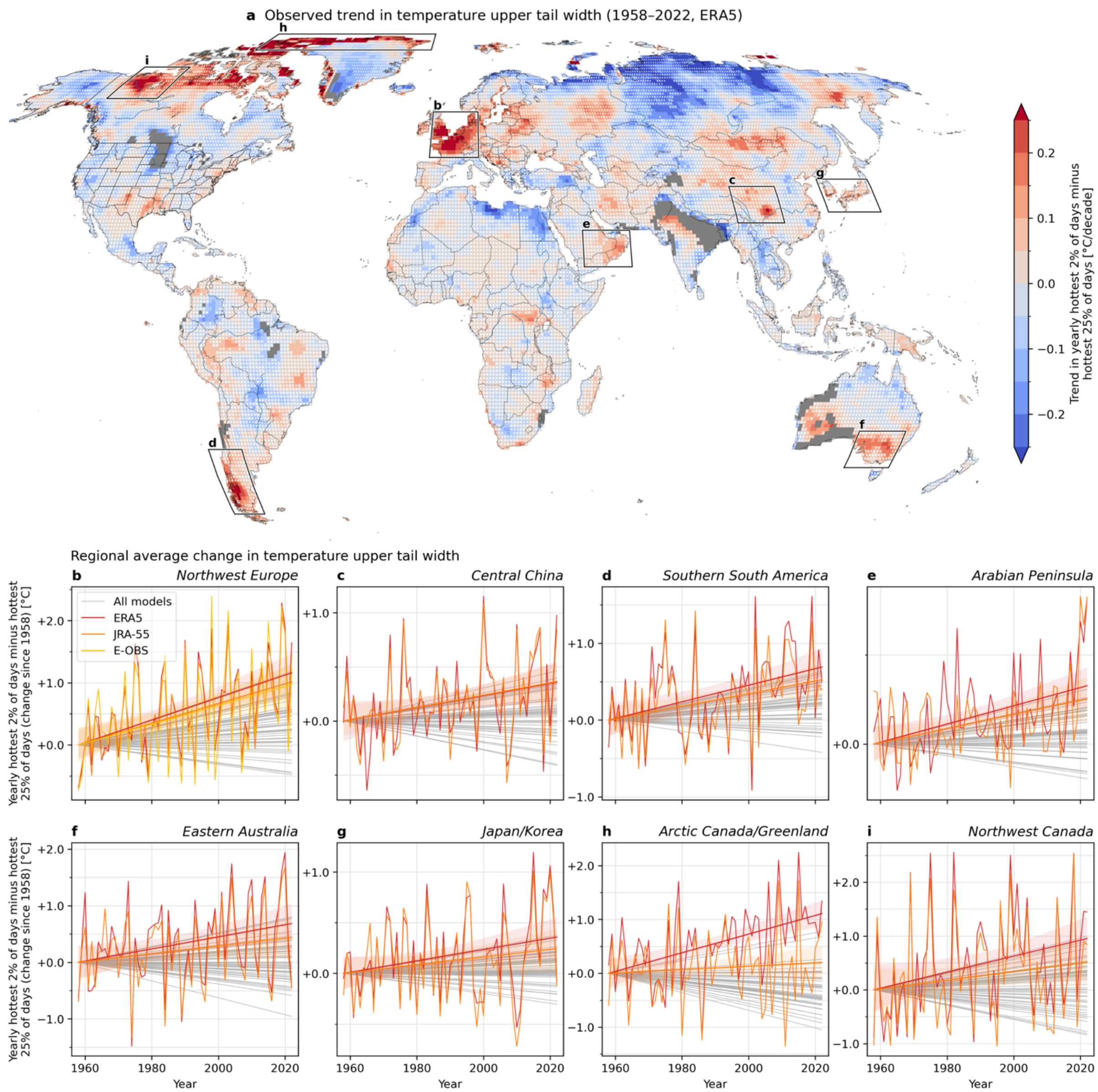


**Figure 2 A global emergence of regional heatwave hotspots.** **a** Global trends in extreme heat tail behaviour, estimated by calculating long term trends in the differences of the yearly 99th percentile of daily maximum temperature (Tx) and the average of the hottest quarter of days of each year (annual 87.5th percentile of Tx as the average of the upper quartile bound by the 75th and 100th percentile) at each grid point over 1958-2022. Areas where trends in the annual hottest quarter of Tx are negative are shown in grey. A warming of the most extreme events exceeding the underlying summer-average warming (i.e., a widening of the upper tail of the temperature distribution) is observed in various regions globally. **b-i** Timeseries and linear trends of regionally-aggregated changes for areas highlighted in **b** using ERA5 (red), JRA-55 (orange) and E-OBS (yellow, for Europe only) including b Europe, c Central China (see labels in a). Grey lines show the trends retrieved from a suite of climate models, which largely fail to reproduce observed trends (see Fig. 3 for further details).

Fig. S1 and the methods section detail the objective selection criteria which motivated the eight regions shown in Fig. 2. These conditions require robust trends across time periods and reanalysis products. Analogous assessments over additional regions that do not meet all of the criteria provided in Fig. S2, S3.

The observed occurrence of hotspots is largely, if not completely, missed over the same regions by state-of-the-art modelling frameworks (Fig. 3a). These areas are indicated in dark red in Fig. 3a. In these regions the observed trends are in the extreme end or even outside of the modelled spread, even when using global mean temperature as covariate instead of time (Fig. S5, S6b, S8). Because these observed trends in extreme temperatures are only compared with modelled trends after removing the average summer warming, model-observation discrepancy resulting from seasonal-scale warming differences is minimized.

Regions such as Northwest Europe (Fig. 1e), Central China and Northeast Canada among other areas have repeatedly witnessed record breaking extreme heat events in recent years and the upper tail of the nearby temperature distribution has steadily been widening (Fig. 2). These large and in part densely populated regions are among those for which we find that the trends in the hottest 2% ($99^{th}$ percentile) of daily maximum temperatures Tx, after accounting for background summer warming, exceed the $95^{th}$ percentile of all the model spread (Fig. 3b-i). Other notable areas where grid-point discrepancies persist but regional averages don't meet all the criteria outlined in Fig. S1 include densely populated areas of the Southern US, and important biomes such as the Amazon and central Africa (Fig. S1-S3).

In the case of Southern South America (Fig. 3d), the Arabian Peninsula (Fig. 3e), and Arctic Canada/Greenland (Fig. 3h) observed trends in ERA5 are stronger than in any model realization. While reanalysis datasets (ERA5, EOBS, JRA-55) agree on sign of trends, is notable that their magnitude differs. JRE-55 shows smaller trends throughout the regions outlined in Fig. 3. In some cases such as over the Arctic (Fig. 3h) or over Northwest Canada (Fig. 3i) these discrepancies can be quite large, to a degree that JRA-55 is more within the model ensemble spread and model-reanalysis differences less significant (i.e. the confidence intervals largely overlap). As ERA5 can be considered the more modern reanalysis, these discrepancies could be explained by difficulties in data assimilation in high latitudes in JRE-55.

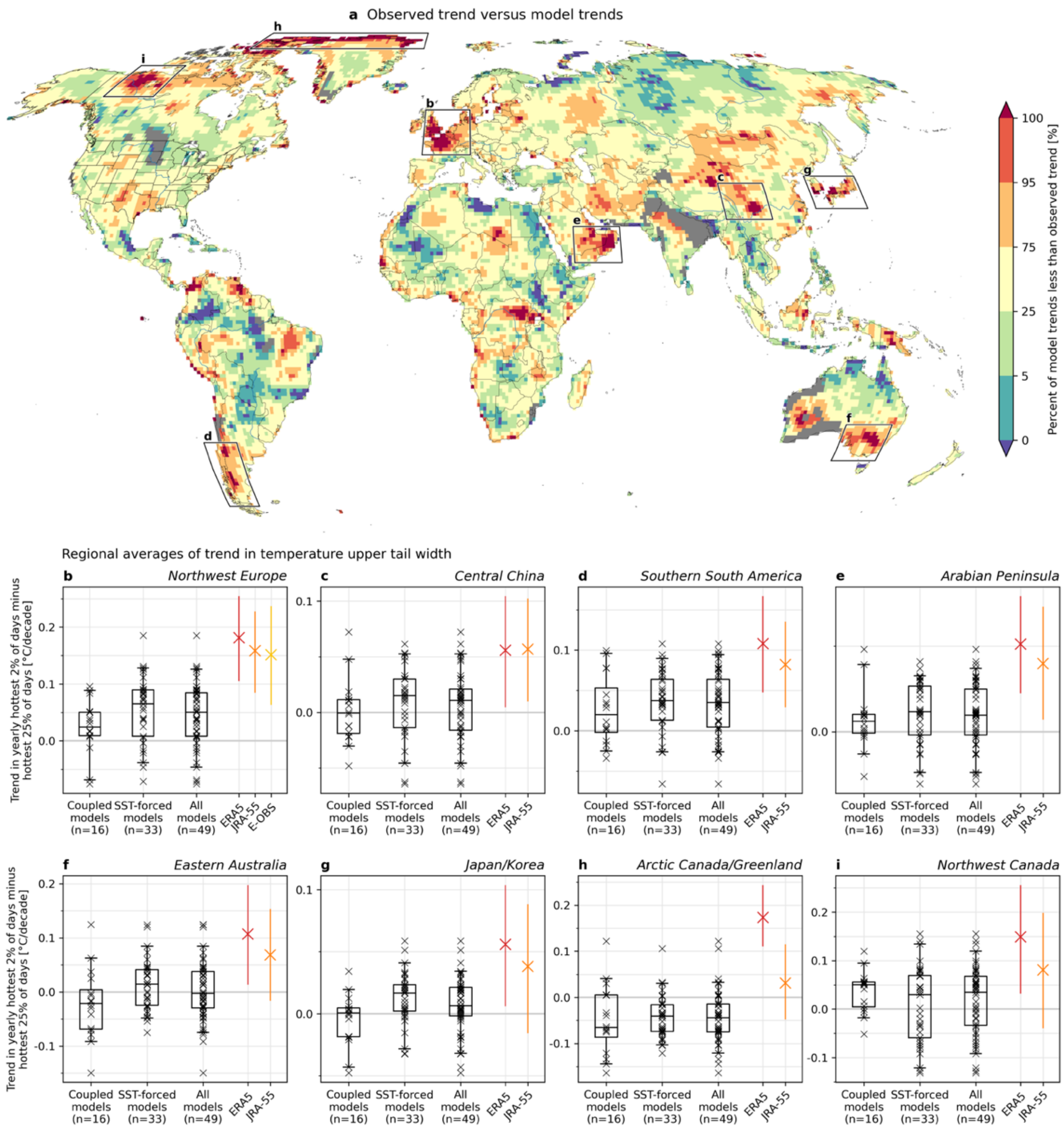


**Figure 3 Regional trends of extreme temperatures are underestimated in climate model experiments in multiple regions globally. a** Comparison of observed trends in tail width (99th percentile minus the 87th percentile) with 49 simulations from climate models of various architectures (see Table S1). Observed trends are outside of the modelled range in several regions globally (dark red). Areas where hottest quarter of Tx shows a negative trend in observations are shown in grey. **b-i** Distributions of modelled trends in the hottest 2% (99th percentile) to the average of the hottest 25% days (87.5th percentile) each year in different model architectures compared to ERA5 (red) and JRE-55 (orange) and (E-OBS, in b only) observation based gridded climate data, displayed as box-and whisker-plots. Boxes display 25th and 75th percentile while the median is shown as a horizontal black line. The whiskers denote the 5th and 95th percentile, while the single model values are provided as scattered x'es and uncertainty bounds are based on bootstrapping.

While the differences between observed and modelled trends in the Northwestern Europe hotspot have been investigated (Faranda et al., 2023; Patterson, 2023; Rousi et al., 2022; Vautard et al., 2023), here we expand such an analysis to the remainder of global land area. In contrast to previous studies, our analysis also includes sea surface temperature (SST)-forced models, to further minimize the sources of discrepancy between models and observed history. We find that model biases are largely independent of the type of model set up, locally (Fig. 3b-i) and on a global scale, where the land area fraction over which trends are misaligned is only slightly reduced in high-resolution (25-50 km) (Fig. S7a-c, Fig. S8a-c) and SST-forced models (Fig, S7d-f, Fig. S8 d-f). In experiments where the atmosphere is forced with observed SSTs, the signal is slightly improved for most hotspot regions, compared to experiments in which atmosphere and oceans are fully coupled and not informed by observed SSTs (see Table S1 for a list of all models investigated), implying a present but minor role for SST pattern forcing of observed trends. We further find that larger SST-forced ensembles (up to a total of 109 model runs) do not offer a substantial improvement for most regions (Fig. S4). For eastern Australia and Japan/Korea (Figs. S4f,g), however trends do exhibit more accurate levels for these forced large Ensembles, suggesting a potential role in SST forced teleconnections in these regions that could have contributed to recent trends.

Finally, we find that discrepancies of strongly positive trends in the upper tails of surface temperature distributions are notable also when aggregated globally or assessed over specific latitudinal ranges (Fig. 4, Fig. S9). While climate models exhibit a higher fraction of land area overall with positive tail width trends than in the observations (55% in models, 48% in ERA5), they simulate a much smaller area of significantly positive trends than seen in observations that are statistically significant to a smaller degree (Fig. S9a, b, d). At $p<0.05$, 16.3% of land-weighted positive trends are significant in ERA5, versus 10.5% in models, and this discrepancy intensifies at higher significance levels (7.9% vs. 3.5% at $p<0.01$) (Fig. S9c, e). Probability density histograms show that models do reproduce the shape of the trend distribution (Fig. 4a), while still underestimating the extreme trends, as indicated by the higher skewness of the observed distribution (Fig. 4a). Interestingly, and not expected, the distribution of low resolution models matches the reanalysis better (skewness of 0.24 and 0.4 respectively) compared to high resolution models (skewness of 0.15), while all models combined exhibit a skewness of 0.2 (Fig. S10a). Low-resolution models also exhibit the strongest single grid-point trends, which may often be attributable to singularities in Arctic regions, in particular in the vicinity of shores. Preliminary analyses (not shown) suggest a role of the cryosphere implementation in these models (see exemplary trend map based on one ensemble member in Fig. S11). The underestimation of positive trends is also expressed by the cumulative probability ratio

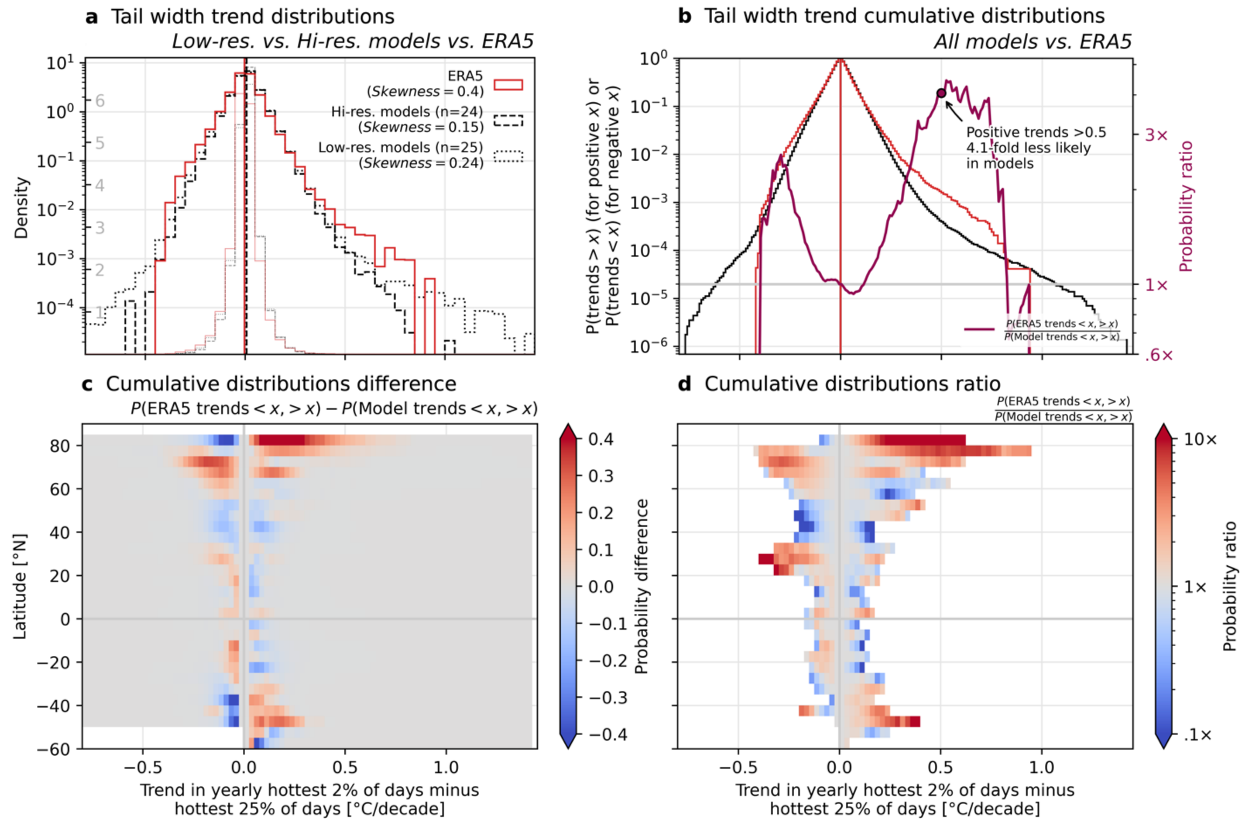


**Figure 4 Global underestimation of trends in extreme temperature tail width in climate models compared to reanalysis data. a** Land weighted probability density histogram of trends in the width of hottest 2% (99[th] percentile) compared to the mean of the upper 25% (87.5[th] percentile) in ERA5 (red), high-resolution climate models (black, dashed) and low-resolution simulations (black, dotted). Number of models included, and the skewness of the distribution is provided in the legend. Histograms are shown with a log-scale (saturated colors) and a linear scale (translucent colors). **b** Cumulative probability distributions and ratios of negative trends (left of zero) and positive trends (right of zero). Models underestimated positive trends exceeding 0.5 °C/decade by a factor of 4.1. **c** Differences in cumulative distribution between reanalysis and models and **d** probability ratios in trends by latitude. Largest discrepancies are identified in northern hemisphere high latitudes and the mid-latitudes of northern and southern hemispheres.

between ERA5 and models (Fig. 4b). We find that models underestimate positive trends exceeding 0.5°C per decade by a factor of 4.1. When assessing cumulative distributions of probability ratios irrespective of the sign this value is found to be 3.5 (Fig. S10b). Biases are found to be strongest in the Northern high latitudes, in both cumulative probability differences (Fig. 4c) and ratios (Fig. 4d), while Northern and Southern Hemisphere midlatitudes, where multiple hotspots are located, are also emphasized. Underestimated Arctic warming in climate models has been reported previously

(Rantanen et al., 2022). Although they assess differences in mean warming, these biases might also affect the tails of the distribution.

**Summary and Discussion**

While coupled climate models have been useful tools in modeling and projecting the past global mean temperature response to anthropogenic activities over the historical period (Hausfather et al., 2020), (Fig, S5), we find that observed long term trends in the tail behavior of extreme heat events are indeed outside of what historical model ensembles suggests in several regions globally (Figs. 3, S4, S7, S8). High impact extreme weather events are almost without exception the outcome of several compounding factors acting together, with regionally varying importance of each component involved.

Dry soils and associated land-atmosphere feedbacks are major heatwave drivers (Barriopedro et al., 2023; Bartusek et al., 2022; Miralles et al., 2014). It has been found that an amplified warming trend of hot days versus mean warming in the tropics can largely be explained by a 'dry gets hotter' mechanism (Byrne, 2021), while precipitation trends were found to govern the occurrence of hot-dry extremes globally (Bevacqua et al., 2022). Huntingford et al. (Huntingford et al., 2024) found regionally varying causes for trends in the upper 90th percentile of daily temperatures: while in the Northern Hemisphere extra-tropics dry soils were emphasized, trends in tropical Africa were linked to increased available energy, estimated from the surface sensible heat to the atmosphere and losses due to evaporation. This is consistent with earlier findings (Urdiales-Flores et al., 2023) that attributed amplified warming in Mediterranean type regions. Simpson et al. (Simpson et al., 2024) found that trends in humidity, which are strongly dependent on the accurate depiction of rainfall patterns (Bevacqua et al., 2022), evaporation (which is partially controlled by vegetation) and hydrological characteristics of the land surface, including vegetation are still not accurately reproduced.

Persistent high-pressure systems, which materialize as local blocking patterns (Kautz et al., 2022) or zonally-elongated stationary Rossby waves (Kornhuber et al., 2019; Petoukhov et al., 2013; White et al., 2022) are important contributors to weather extremes especially in the mid-latitudes (Screen & Simmonds, 2014). Atmospheric circulation is considered a major source of uncertainty which also affects precipitation trends (Shepherd, 2014) consequential for surface drying, energy balances and temperatures. Specifically Europe has been identified as a global heatwave hotspot (Rousi et al., 2022). Here hottest days are warming twice as fast as mean summer days (Patterson, 2023), a trend that is driven by atmosphere dynamical patterns (Faranda et al., 2023; Rousi et al., 2022) and is largely missed by climate models (Vautard et al., 2023).

Although the newest generation of climate models shows some improvement in the representation of the frequency and magnitude of atmospheric blocking (Kautz et al., 2022; Schiemann et al., 2020; Woollings et al., 2018), these measures are still underestimated in CMIP6 models (Davini & D'Andrea, 2020). Recent research has shown that while models do accurately reproduce the location and strength of upper-level wave patterns, they also substantially underestimate the surface response to quasi-stationary wave patterns of the type involved in several of recent extreme weather events, e.g. the European heatwave of 2003 (Kornhuber et al., 2023; Luo et al., 2022).

The slight improvement we find in SST-forced models in particular for Eastern Australia and Japan / Korea provides further evidence for a potential role for specific SST patterns (Fig. S4) in forcing certain atmospheric dynamical circulation patterns and/or rainfall patterns and associated land-atmosphere feedbacks, which have played an important role in recent high-impact heatwaves (Di Capua et al., 2021; Duchez et al., 2016; Kornhuber et al., 2019; Rousi et al., 2023). Heatwaves in North America are often linked to persistent ridges in the Jetstream, which have been related to SST patterns in the Pacific (McKinnon et al., 2016a; Swain et al., 2016). Persistent and extreme heat has particularly increased over western and southern North America (S. E. Perkins-Kirkpatrick & Lewis, 2020; Rousi et al., 2022). Tropical Pacific SSTs exert a powerful control on climate and weather variability worldwide, primarily via El Niño-Southern Oscillation (ENSO) cycles. El Niño has been suggested out as a potential contributor to some extreme heat and precipitation in the Northern mid-latitudes in summer 2023 (S. Perkins-Kirkpatrick et al., 2024). Further, it is known that a La Niña-like SST trend in the tropical Pacific has contributed to the two-decades-long megadrought in southwest North America (Seager et al., 2023). ENSO events also have an important role in favoring specific heat extremes such as the 2010 heatwave in Russia which was associated with a La Niña-like SST pattern (Di Capua et al., 2021). State-of-the-art climate models predict that rising GHGs should reduce the west-to-east warm-to-cool SST gradient across the equatorial Pacific while, in observations, the gradient has strengthened over recent decades along with rising GHG concentrations (Seager et al., 2019, 2022). Regional biases in heatwave intensification may therefore be partially linked to diverging SST signals in models and observations and how they teleconnect to precipitation and temperature worldwide. However, since biases persist nearly entirely in SST-forced experiments this cannot be the sole explanation (Fig. 3, Fig. S4).

The representation of aerosols and their interaction with clouds remain a major challenge for climate models (Lee et al., 2016), but these factors can play an important role for regional heatwave trends (Wang et al., 2023). Aerosol reduction has been identified as a contributing driver of European heat wave trends, largely missed by regional models (Schumacher et al., 2024). China has substantially in reduced aerosol and ozone precursors in recent years, which have contributed to increased local temperature trends in some locations (Gao et al., 2022).

**Conclusion**

Actionable climate assessment for effective climate adaptation and mitigation requires skillful and reliable projections of extreme weather risks under different emission scenarios on a regional to local level. This holds particularly for the representation of recently observed extreme-extremes that might be rare under current climatic conditions but will become more likely under continued greenhouse gas emissions (GHG) (S. E. Perkins-Kirkpatrick & Lewis, 2020; Thompson et al., 2023). Skillful projections of trends in extreme-extremes (unprecedented or record-shattering extremes) must build on a thorough physical understanding of why they are emerging and the nonlinear behavior responsible so that model simulations can be benchmarked, and potential biases can be accounted for.

In large and densely-populated areas such as western Europe and China, and other areas that feature important biomes for the world climate such as the Amazon, the Congo basin and polar regions around Greenland and Canada, some of which have been discussed in the context of climate tipping points (Armstrong McKay et al., 2022; Lenton et al., 2008), the multi-model mean does not show the enhanced warming of the temperature distributions' upper tails observed in these regions (Fig, 1, Fig. S4). Note that the multi-model mean is often used and prioritized in many assessments of climate risks, while upper percentiles are often treated as implausible scenarios and are at times rejected as freak outliers. For instance, the 1.5 °C warming target established by the Paris Agreement was set largely based on avoiding "dangerous climate change", in part associated with critical tipping elements and/or thresholds in the Earth system (Armstrong McKay et al., 2022; Schellnhuber et al., 2016). However, if impacts of global warming, such as amplified extreme heat, proceed faster than expected based on multi-model mean projections that justify such a warming target, its utility may deserve reconsideration. We find that in numerous regions (Fig. 2, 3), trends in observations over the past 65 years even exceed the 95$^{th}$ percentile of the model spread and, in some cases, even exceed the 100th percentile and are entirely outside of the modelled range irrespective of any model configuration investigated here. These findings hold for model simulations at higher resolution, or forced with historical SSTs, as well as with greatly expanded ensemble sizes (Figs. S4, S7, S8).

Newer modelling initiatives such as super high-resolution frameworks suggested e.g. in the Earth Virtualization Engine (EVE) (Stevens et al., 2023) promise convection permitting resolution and offer possibilities in improving the depiction of important mechanisms. Such mechanisms may include processes that link SSTs with Rossby waves and associated extremes (Teng et al., 2022), regional blocking and realistic surface response of heat events to such atmospheric patterns (Kornhuber et al., 2023; Luo et al., 2022). Newer generation models have also shown an improved skill in modelling blocking events which is more pronounced in high resolution models (Harvey et al., 2020; Schiemann et al., 2020). Given the importance of non-linear feedbacks involving hydroclimatic processes, a proper representation of the seasonal relationships of the flow of energy and water in the soil-vegetation-atmosphere continuum needs to be assured (Gloege et al., 2022). Reasonable forecasts of past extreme heatwaves suggests that models can in principle produce such extreme-extremes when directly forced with the correct boundary conditions (Holley & Lee, 2022; White et al., 2023). Ensemble boosting techniques can be used to create large ensembles of extraordinary extremes at reduced computational cost (Fischer et al., 2023; Ragone et al., 2018). In an evolutionary manner, these algorithms filter out runs that will result in conditions while preserving those that follow an extreme trajectory. This allows a sampling around a specific event characteristic. A large ensemble of highly anomalous events, which would be featured only at an extremely low rate in large ensembles (McKinnon & Simpson, 2022), allows for an in-depth and statistically robust analysis of the governing physics of 'extreme-extremes' in models.

Further, ML approaches have shown promising results for providing more reliable bias adjustment of climate model output (Hess et al., 2023). These are based on methods from image processing and are better in retaining the relationships between variables compared to more traditional quantile-mapping approaches. This is particularly important when analysing risks and impacts from compound extremes. Machine learning (ML) techniques could also assist in detecting nonlinear and regime changing behaviour, where common drivers experience a stronger coupling and dependence structures - i.e. the relationships of important variables such as soil moisture, pressure and temperature - are dominantly driven by feedbacks (Bartusek et al., 2022; Lesk et al., 2021). Recent advances in ML-driven weather forecasts exemplify the potential in climate modelling (Bi et al., 2023; Lam et al., 2023) to offer more accurate and less computationally-costly avenues for resolving important sub-grid processes (Schneider et al., 2023; Yuval & O'Gorman, 2020), compared to purely numerical approaches. New assimilation techniques that integrate observational datasets and exploit advanced interpolation frameworks have been proven to improve the depiction of extremes compared to reanalysis datasets (Funk et al., 2019), and provide climate information at a higher resolution.

While our findings provide many avenues for interesting and relevant new research the authors stress that the best way to reduce both uncertainty in and exposure to climate impacts is a rapid transition of relevant societal sectors away from fossil fuels to stabilize global temperature rise.

## Data & Methods

**Data:** The analysis is based on daily-maximum temperature (Tx) at 2-meter height. All model-derived results in the main analysis use data from the HighResMIP project (Haarsma et al., 2016), which provides a good balance and coherent set-up of coupled and SST-forced experiments. Within HighResMIP, configurations labeled "SST-forced" in Table S1 refer to a concatenation of the "highresSST-present" experiment from 1958–2014 with the "highresSST-future" experiment from 2015–2022 (with matching member IDs only). Both are atmosphere-only, with "highresSST-present" forced by historic SST/sea-ice fields and "highresSST-future" forced by SSP585 SST/sea-ice fields. Configurations labeled "Coupled" in the table above refer to a concatenation of the "hist-1950" experiment from 1950–2014 with the "highres-future" experiment from 2015–2022 (with matching member IDs only). Both are coupled, with "hist-1950" subject to historical forcing and "highres-future" subject to SSP585 forcing. All model data were pre-processed with *xmip* to standardize metadata and data structures.

ERA5 reanalysis data (Hersbach et al., 2020) from years 1958–2023 were used in Figure 1 to display 2-meter Tx and ERA5 u and v components of wind at the 300 hPa pressure level and were downloaded from the Copernicus Data Store (https://cds.climate.copernicus.eu/#!/home). For Figures 2 the data was limited to 1958 – 2022 as a global analysis requires the availability of the entire annual dataset.

Six hourly temperature data from the Japanese 55-year Reanalysis (JRA-55) (Kobayashi et al., 2015) ranging from years 1958-2022 were used in Figures 2 and Figures 3 and were retrieved from https://jra.kishou.go.jp/JRA-55/index_en.html

Temperature data from the gridded E-OBS (Cornes et al., 2018) were used for calculating trends over Europe as shown in Fig. 2b and Fig. 3b and were downloaded from: https://www.ecad.eu/download/ensembles/download.php

**Methods:** Tx is defined as the hottest daily temperature based on 6-hourly data. In the main analysis, the yearly 99th and 87.5th percentiles (as the median of the upper quartile 75th to 100th percentile) of Tx were calculated for each grid-point from model runs (on their native grids) and ERA5, for all years 1958–2022. The 99th percentile represents the median day of the hottest 2% days of the year , while the 87.5th percentile approximates the average summer day, as it represents the median of the hottest quarter of days of the year. This percentile approach is therefore generalizable to all areas of the globe, not dependent on specific calendar definitions of seasons. Computed percentiles were conservatively regridded to a common 1-degree grid using *xesmf*. We compute linear trends in the yearly difference of these two percentiles, similar to a quantile regression approach (Haugen et al., 2018; McKinnon et al., 2016b). In Figures 2 and 3, significance and uncertainty ranges for observed trends are calculated via a bootstrap approach. In Figure 2a, for each grid point, the 65 yearly datapoints (the difference between yearly 99t and 87.th percentile Tx) from 1958 to 2022 were resampled 1,000 times (with replacement, and without shuffling in time), calculating a linear trend in time for each iteration, and grid points were covered with a white dot if the 2.5th to 97.5th percentile range of these trend values crossed zero. In Figure 2b–i, for each region, a regional mean was calculated each year of the difference between the yearly 99th and 87.5th percentile Tx at each grid point, the resulting 65 yearly datapoints were resampled 10,000 times as described above, and the 2.5th to 97.5th percentile range in the iterations' trend values is shown as a vertical red line. Regions shown in Fig. 2 and Fig. 3 were selected based on a set of conditions outlined in Fig. S1: the trend of the regional average is positive and significant ($p < 0.05$) in ERA5 over the period 1958 - 2022, positive in JRA55 over the period 1958 – 2022 and positive over the period 1980 – 2022 in all available datasets. Those regions are marked black in Fig. S1. And regional average trends are shown in Figs. S2 and S3. In Fig. S9 (and where it is referenced in the main text), p-values for both ERA5 and model data are calculated parametrically, via a two-tailed Wald Test with a t-distribution of the test statistic, rather than applying the full iterative bootstrapping approach to all model ensemble members (in contrast to the significance testing in Fig. 2 and 3).

**Data Availability:** All model data was accessed through ESGF (https://aims2.llnl.gov/search). All model runs in main analysis are from CMIP6's HighResMIP (https://gmd.copernicus.org/articles/9/4185/2016/gmd-9-4185-2016.html). All model runs listed in Table S1 are available from ESGF (hosted at the LLNL data node) at the time of accessing, given matching member IDs across historical and future experiments, and with uninterrupted data across the entire 1958–2023 period, were used. ERA5 data was downloaded from the Copernicus Climate Data Store.

**Code availability** All figures were produced using Python v.3.6 (https://www.python.org/downloads/release/python-360/). All code needed to reproduce the main figures will be made available before publication.

**Acknowledgements:** The authors want to thank the ECMWF and the Copernicus Climate Change Service for providing the ERA5 reanalysis and World Climate Research Programme, which, through its Working Group on Coupled Modelling, coordinated and promoted CMIP6. We thank the climate modeling groups for producing and making available their model output, the Earth System Grid Federation (ESGF) for archiving the data and providing access, and the multiple funding agencies who support CMIP6 and ESGF.

**Author Contributions:** K.K. wrote the first draft of the manuscript, and conceived and designed the research. S.B. analyzed the data. S.B., R.S., M.T., H.J.S. helped with designing the research and with the writing of the manuscript.

**Funding Information:** K.K. was supported by the German Federal Ministry of Education and Research within the ClimXtreme project subprojects PERSEVERE (01LP2322D). R.S. and M.T. were supported by NOAA award NA20OAR4310379 and RS additionally by NSF award AGS-2127684. S.B. was supported by the National Aeronautics and Space Administration (NASA) under the Future Investigators in NASA Earth and Space Science and Technology (FINESST) program, grant 21-EARTH21-0134.

**Competing Interests:** The authors declare no competing interests.

**References:**

Armstrong McKay, D. I., Staal, A., Abrams, J. F., Winkelmann, R., Sakschewski, B., Loriani, S., Fetzer, I., Cornell, S. E., Rockström, J., & Lenton, T. M. (2022). Exceeding 1.5°C global warming could trigger multiple climate tipping points. *Science*, *377*(6611), eabn7950. https://doi.org/10.1126/science.abn7950

Ballester, J., Quijal-Zamorano, M., Méndez Turrubiates, R. F., Pegenaute, F., Herrmann, F. R., Robine, J. M., Basagaña, X., Tonne, C., Antó, J. M., & Achebak, H. (2023). Heat-related mortality in Europe during the summer of 2022. *Nature Medicine*, *29*(7), 1857–1866. https://doi.org/10.1038/s41591-023-02419-z

Barriopedro, D., Fischer, E. M., Luterbacher, J., Trigo, R. M., & García-Herrera, R. (2011). The Hot Summer of 2010: Redrawing the Temperature Record Map of Europe. *Science*, *332*(6026), 220–224. https://doi.org/10.1126/science.1201224

Barriopedro, D., García-Herrera, R., Ordóñez, C., Miralles, D. G., & Salcedo-Sanz, S. (2023). Heat Waves: Physical Understanding and Scientific Challenges. *Reviews of Geophysics*, *61*(2), e2022RG000780. https://doi.org/10.1029/2022RG000780

Bartusek, S., Kornhuber, K., & Ting, M. (2022). 2021 North American heatwave amplified by climate change-driven nonlinear interactions. *Nature Climate Change*, *12*(12), 1143–1150. https://doi.org/10.1038/s41558-022-01520-4

Bathiany, S., Dakos, V., Scheffer, M., & Lenton, T. M. (2018). Climate models predict increasing temperature variability in poor countries. *Science Advances*, *4*(5), eaar5809. https://doi.org/10.1126/sciadv.aar5809

Bevacqua, E., Zappa, G., Lehner, F., & Zscheischler, J. (2022). Precipitation trends determine future occurrences of compound hot–dry events. *Nature Climate Change*, *12*(4), 350–355. https://doi.org/10.1038/s41558-022-01309-5

Bi, K., Xie, L., Zhang, H., Chen, X., Gu, X., & Tian, Q. (2023). Accurate medium-range global weather forecasting with 3D neural networks. *Nature*, *619*(7970), 533–538. https://doi.org/10.1038/s41586-023-06185-3

Byrne, M. P. (2021). Amplified warming of extreme temperatures over tropical land. *Nature Geoscience*, *14*(11), 837–841. https://doi.org/10.1038/s41561-021-00828-8

Cornes, R. C., van der Schrier, G., van den Besselaar, E. J. M., & Jones, P. D. (2018). An Ensemble Version of the E-OBS Temperature and Precipitation Data Sets. *Journal of Geophysical Research: Atmospheres*, *123*(17), 9391–9409. https://doi.org/10.1029/2017JD028200

Davini, P., & D'Andrea, F. (2020). From CMIP3 to CMIP6: Northern Hemisphere Atmospheric Blocking Simulation in Present and Future Climate. *Journal of Climate*, *33*(23), 10021–10038. https://doi.org/10.1175/JCLI-D-19-0862.1

Di Capua, G., Sparrow, S., Kornhuber, K., Rousi, E., Osprey, S., Wallom, D., van den Hurk, B., & Coumou, D. (2021). Drivers behind the summer 2010 wave train leading to Russian heatwave and Pakistan flooding. *Npj Climate and Atmospheric Science*, *4*(1), 55. https://doi.org/10.1038/s41612-021-00211-9

Donat, M. G., Pitman, A. J., & Seneviratne, S. I. (2017). Regional warming of hot extremes accelerated by surface energy fluxes. *Geophysical Research Letters*, *44*(13), 7011–7019. https://doi.org/10.1002/2017GL073733

Duchez, A., Frajka-Williams, E., Josey, S. A., Evans, D. G., Grist, J. P., Marsh, R., McCarthy, G. D., Sinha, B., Berry, D. I., & Hirschi, J. J.-M. (2016). Drivers of exceptionally cold North Atlantic Ocean temperatures and their link to the 2015 European heat wave.

*Environmental Research Letters*, *11*(7), 074004. https://doi.org/10.1088/1748-9326/11/7/074004

Faranda, D., Messori, G., Jezequel, A., Vrac, M., & Yiou, P. (2023). Atmospheric circulation compounds anthropogenic warming and impacts of climate extremes in Europe. *Proceedings of the National Academy of Sciences*, *120*(13), e2214525120. https://doi.org/10.1073/pnas.2214525120

Fischer, E. M., Beyerle, U., Bloin-Wibe, L., Gessner, C., Humphrey, V., Lehner, F., Pendergrass, A. G., Sippel, S., Zeder, J., & Knutti, R. (2023). Storylines for unprecedented heatwaves based on ensemble boosting. *Nature Communications*, *14*(1), 4643. https://doi.org/10.1038/s41467-023-40112-4

Fischer, E. M., & Schär, C. (2010). Consistent geographical patterns of changes in high-impact European heatwaves. *Nature Geoscience*, *3*(6), 398–403. https://doi.org/10.1038/ngeo866

Fischer, E. M., Sippel, S., & Knutti, R. (2021). Increasing probability of record-shattering climate extremes. *Nature Climate Change*, *11*(8), 689–695. https://doi.org/10.1038/s41558-021-01092-9

Funk, C., Peterson, P., Peterson, S., Shukla, S., Davenport, F., Michaelsen, J., Knapp, K. R., Landsfeld, M., Husak, G., Harrison, L., Rowland, J., Budde, M., Meiburg, A., Dinku, T., Pedreros, D., & Mata, N. (2019). A High-Resolution 1983–2016 Tmax Climate Data Record Based on Infrared Temperatures and Stations by the Climate Hazard Center. *Journal of Climate*, *32*(17), 5639–5658. https://doi.org/10.1175/JCLI-D-18-0698.1

Gao, J., Yang, Y., Wang, H., Wang, P., Li, H., Li, M., Ren, L., Yue, X., & Liao, H. (2022). Fast climate responses to emission reductions in aerosol and ozone precursors in China during 2013–2017. *Atmospheric Chemistry and Physics*, *22*(11), 7131–7142. https://doi.org/10.5194/acp-22-7131-2022

Gloege, L., Kornhuber, K., Skulovich, O., Pal, I., Zhou, S., Ciais, P., & Gentine, P. (2022). Land-Atmosphere Cascade Fueled the 2020 Siberian Heatwave. *AGU Advances*, *3*(6), e2021AV000619. https://doi.org/10.1029/2021AV000619

Haarsma, R. J., Roberts, M. J., Vidale, P. L., Senior, C. A., Bellucci, A., Bao, Q., Chang, P., Corti, S., Fučkar, N. S., Guemas, V., von Hardenberg, J., Hazeleger, W., Kodama, C., Koenigk, T., Leung, L. R., Lu, J., Luo, J.-J., Mao, J., Mizielinski, M. S., … von Storch, J.-S. (2016). High Resolution Model Intercomparison Project (HighResMIP v1.0) for CMIP6. *Geoscientific Model Development*, *9*(11), 4185–4208. https://doi.org/10.5194/gmd-9-4185-2016

Harvey, B. J., Cook, P., Shaffrey, L. C., & Schiemann, R. (2020). The Response of the Northern Hemisphere Storm Tracks and Jet Streams to Climate Change in the CMIP3, CMIP5, and CMIP6 Climate Models. *Journal of Geophysical Research: Atmospheres*, *125*(23), e2020JD032701. https://doi.org/10.1029/2020JD032701

Haugen, M. A., Stein, M. L., Moyer, E. J., & Sriver, R. L. (2018). Estimating Changes in Temperature Distributions in a Large Ensemble of Climate Simulations Using Quantile Regression. *Journal of Climate*, *31*(20), 8573–8588. https://doi.org/10.1175/JCLI-D-17-0782.1

Hausfather, Z., Drake, H. F., Abbott, T., & Schmidt, G. A. (2020). Evaluating the Performance of Past Climate Model Projections. *Geophysical Research Letters*, *47*(1), e2019GL085378. https://doi.org/10.1029/2019GL085378

Hersbach, H., Bell, B., Berrisford, P., Hirahara, S., Horányi, A., Muñoz-Sabater, J., Nicolas, J., Peubey, C., Radu, R., Schepers, D., Simmons, A., Soci, C., Abdalla, S., Abellan, X., Balsamo, G., Bechtold, P., Biavati, G., Bidlot, J., Bonavita, M., … Thépaut, J. (2020). The ERA5 global reanalysis. *Quarterly Journal of the Royal Meteorological Society*, *146*(730), 1999–2049. https://doi.org/10.1002/qj.3803

Hess, P., Lange, S., Schötz, C., & Boers, N. (2023). Deep Learning for Bias-Correcting CMIP6-Class Earth System Models. *Earth's Future*, *11*(10), e2023EF004002. https://doi.org/10.1029/2023EF004002

Holley, D., & Lee, S. H. (2022). Forecasting extreme heat in the UK during July 2022. *Weather*, *77*(9), 320–321. https://doi.org/10.1002/wea.4290

Huntingford, C., Cox, P. M., Ritchie, P. D. L., Clarke, J. J., Parry, I. M., & Williamson, M. S. (2024). Acceleration of daily land temperature extremes and correlations with surface energy fluxes. *Npj Climate and Atmospheric Science*, *7*(1), 84. https://doi.org/10.1038/s41612-024-00626-0

Intergovernmental Panel on Climate Change. (2023). *Climate Change 2021 – The Physical Science Basis: Working Group I Contribution to the Sixth Assessment Report of the Intergovernmental Panel on Climate Change* (1st ed.). Cambridge University Press. https://doi.org/10.1017/9781009157896

Kautz, L.-A., Martius, O., Pfahl, S., Pinto, J. G., Ramos, A. M., Sousa, P. M., & Woollings, T. (2022). Atmospheric blocking and weather extremes over the Euro-Atlantic sector – a review. *Weather and Climate Dynamics*, *3*(1), 305–336. https://doi.org/10.5194/wcd-3-305-2022

Kobayashi, S., Ota, Y., Harada, Y., Ebita, A., Moriya, M., Onoda, H., Onogi, K., Kamahori, H., Kobayashi, C., Endo, H., Miyaoka, K., & Takahashi, K. (2015). The JRA-55 Reanalysis: General Specifications and Basic Characteristics. *Journal of the Meteorological Society of Japan. Ser. II*, *93*(1), 5–48. https://doi.org/10.2151/jmsj.2015-001

Kornhuber, K., Lesk, C., Schleussner, C. F., Jägermeyr, J., Pfleiderer, P., & Horton, R. M. (2023). Risks of synchronized low yields are underestimated in climate and crop model projections. *Nature Communications*, *14*(1), 3528. https://doi.org/10.1038/s41467-023-38906-7

Kornhuber, K., Osprey, S., Coumou, D., Petri, S., Petoukhov, V., Rahmstorf, S., & Gray, L. (2019). Extreme weather events in early summer 2018 connected by a recurrent hemispheric wave-7 pattern. *Environmental Research Letters*, *14*(5), 054002. https://doi.org/10.1088/1748-9326/ab13bf

Lam, R., Sanchez-Gonzalez, A., Willson, M., Wirnsberger, P., Fortunato, M., Alet, F., Ravuri, S., Ewalds, T., Eaton-Rosen, Z., Hu, W., Merose, A., Hoyer, S., Holland, G., Vinyals, O., Stott, J., Pritzel, A., Mohamed, S., & Battaglia, P. (2023). Learning skillful medium-range global weather forecasting. *Science*, *382*(6677), 1416–1421. https://doi.org/10.1126/science.adi2336

Lee, L. A., Reddington, C. L., & Carslaw, K. S. (2016). On the relationship between aerosol model uncertainty and radiative forcing uncertainty. *Proceedings of the National Academy of Sciences*, *113*(21), 5820–5827. https://doi.org/10.1073/pnas.1507050113

Lenton, T. M., Held, H., Kriegler, E., Hall, J. W., Lucht, W., Rahmstorf, S., & Schellnhuber, H. J. (2008). Tipping elements in the Earth's climate system. *Proceedings of the National Academy of Sciences*, *105*(6), 1786–1793. https://doi.org/10.1073/pnas.0705414105

Luo, F., Selten, F., Wehrli, K., Kornhuber, K., Le Sager, P., May, W., Reerink, T., Seneviratne, S. I., Shiogama, H., Tokuda, D., Kim, H., & Coumou, D. (2022). Summertime Rossby waves in climate models: Substantial biases in surface imprint associated with small biases in upper-level circulation. *Weather and Climate Dynamics*, *3*(3), 905–935. https://doi.org/10.5194/wcd-3-905-2022

McKinnon, K. A., Rhines, A., Tingley, M. P., & Huybers, P. (2016a). Long-lead predictions of eastern United States hot days from Pacific sea surface temperatures. *Nature Geoscience*, *9*(5), 389–394. https://doi.org/10.1038/ngeo2687

McKinnon, K. A., Rhines, A., Tingley, M. P., & Huybers, P. (2016b). The changing shape of Northern Hemisphere summer temperature distributions. *Journal of Geophysical Research: Atmospheres*, *121*(15), 8849–8868. https://doi.org/10.1002/2016JD025292

McKinnon, K. A., & Simpson, I. R. (2022). How Unexpected Was the 2021 Pacific Northwest Heatwave? *Geophysical Research Letters*, *49*(18), e2022GL100380. https://doi.org/10.1029/2022GL100380

Miralles, D. G., Teuling, A. J., van Heerwaarden, C. C., & Vilà-Guerau de Arellano, J. (2014). Mega-heatwave temperatures due to combined soil desiccation and atmospheric heat accumulation. *Nature Geoscience*, *7*(5), 345–349. https://doi.org/10.1038/ngeo2141

Mitchell, D., Kornhuber, K., Huntingford, C., & Uhe, P. (2019). The day the 2003 European heatwave record was broken. *The Lancet Planetary Health*, *3*(7), e290–e292. https://doi.org/10.1016/S2542-5196(19)30106-8

Overland, J. E., & Wang, M. (2021). The 2020 Siberian heat wave. *International Journal of Climatology*, *41*(S1). https://doi.org/10.1002/joc.6850

Patterson, M. (2023). North-West Europe Hottest Days Are Warming Twice as Fast as Mean Summer Days. *Geophysical Research Letters*, *50*(10), e2023GL102757. https://doi.org/10.1029/2023GL102757

Perkins-Kirkpatrick, S., Barriopedro, D., Jha, R., Wang, L., Mondal, A., Libonati, R., & Kornhuber, K. (2024). Extreme terrestrial heat in 2023. *Nature Reviews Earth & Environment*, *5*(4), 244–246. https://doi.org/10.1038/s43017-024-00536-y

Perkins-Kirkpatrick, S. E., & Lewis, S. C. (2020). Increasing trends in regional heatwaves. *Nature Communications*, *11*(1), 3357. https://doi.org/10.1038/s41467-020-16970-7

Petoukhov, V., Rahmstorf, S., Petri, S., & Schellnhuber, H. J. (2013). Quasiresonant amplification of planetary waves and recent Northern Hemisphere weather extremes. *Proceedings of the National Academy of Sciences*, *110*(14), 5336–5341. https://doi.org/10.1073/pnas.1222000110

Ragone, F., Wouters, J., & Bouchet, F. (2018). Computation of extreme heat waves in climate models using a large deviation algorithm. *Proceedings of the National Academy of Sciences*, *115*(1), 24–29. https://doi.org/10.1073/pnas.1712645115

Rantanen, M., Karpechko, A. Yu., Lipponen, A., Nordling, K., Hyvärinen, O., Ruosteenoja, K., Vihma, T., & Laaksonen, A. (2022). The Arctic has warmed nearly four times faster than the globe since 1979. *Communications Earth & Environment*, *3*(1), 168. https://doi.org/10.1038/s43247-022-00498-3

Robinson, A., Lehmann, J., Barriopedro, D., Rahmstorf, S., & Coumou, D. (2021). Increasing heat and rainfall extremes now far outside the historical climate. *Npj Climate and Atmospheric Science*, *4*(1), 45. https://doi.org/10.1038/s41612-021-00202-w

Rousi, E., Fink, A. H., Andersen, L. S., Becker, F. N., Beobide-Arsuaga, G., Breil, M., Cozzi, G., Heinke, J., Jach, L., Niermann, D., Petrovic, D., Richling, A., Riebold, J., Steidl, S., Suarez-Gutierrez, L., Tradowsky, J. S., Coumou, D., Düsterhus, A., Ellsäßer, F., … Xoplaki, E. (2023). The extremely hot and dry 2018 summer in central and northern Europe from a multi-faceted weather and climate perspective. *Natural Hazards and Earth System Sciences*, *23*(5), 1699–1718. https://doi.org/10.5194/nhess-23-1699-2023

Rousi, E., Kornhuber, K., Beobide-Arsuaga, G., Luo, F., & Coumou, D. (2022). Accelerated western European heatwave trends linked to more-persistent double jets over Eurasia. *Nature Communications*, *13*(1), 3851. https://doi.org/10.1038/s41467-022-31432-y

Schär, C., Vidale, P. L., Lüthi, D., Frei, C., Häberli, C., Liniger, M. A., & Appenzeller, C. (2004). The role of increasing temperature variability in European summer heatwaves. *Nature*, *427*(6972), 332–336. https://doi.org/10.1038/nature02300

Schellnhuber, H. J., Rahmstorf, S., & Winkelmann, R. (2016). Why the right climate target was agreed in Paris. *Nature Climate Change*, *6*(7), 649–653. https://doi.org/10.1038/nclimate3013

Schiemann, R., Athanasiadis, P., Barriopedro, D., Doblas-Reyes, F., Lohmann, K., Roberts, M. J., Sein, D. V., Roberts, C. D., Terray, L., & Vidale, P. L. (2020). Northern Hemisphere blocking simulation in current climate models: Evaluating progress from the Climate Model Intercomparison Project Phase 5 to 6 and sensitivity to resolution. *Weather and Climate Dynamics*, *1*(1), 277–292. https://doi.org/10.5194/wcd-1-277-2020

Schneider, T., Behera, S., Boccaletti, G., Deser, C., Emanuel, K., Ferrari, R., Leung, L. R., Lin, N., Müller, T., Navarra, A., Ndiaye, O., Stuart, A., Tribbia, J., & Yamagata, T. (2023). Harnessing AI and computing to advance climate modelling and prediction. *Nature Climate Change*, *13*(9), 887–889. https://doi.org/10.1038/s41558-023-01769-3

Schumacher, D. L., Singh, J., Hauser, M., Fischer, E. M., Wild, M., & Seneviratne, S. I. (2024). Exacerbated summer European warming not captured by climate models neglecting long-term aerosol changes. *Communications Earth & Environment*, *5*(1), 182. https://doi.org/10.1038/s43247-024-01332-8

Screen, J. A. (2014). Arctic amplification decreases temperature variance in northern mid- to high-latitudes. *Nature Climate Change*, *4*(7), 577–582. https://doi.org/10.1038/nclimate2268

Screen, J. A., & Simmonds, I. (2014). Amplified mid-latitude planetary waves favour particular regional weather extremes. *Nature Climate Change*, *4*(8), 704–709. https://doi.org/10.1038/nclimate2271

Seager, R., Cane, M., Henderson, N., Lee, D.-E., Abernathey, R., & Zhang, H. (2019). Strengthening tropical Pacific zonal sea surface temperature gradient consistent with rising greenhouse gases. *Nature Climate Change*, *9*(7), 517–522. https://doi.org/10.1038/s41558-019-0505-x

Seager, R., Henderson, N., & Cane, M. (2022). Persistent Discrepancies between Observed and Modeled Trends in the Tropical Pacific Ocean. *Journal of Climate*, *35*(14), 4571–4584. https://doi.org/10.1175/JCLI-D-21-0648.1

Seager, R., Ting, M., Alexander, P., Liu, H., Nakamura, J., Li, C., & Newman, M. (2023). Ocean-forcing of cool season precipitation drives ongoing and future decadal drought in southwestern North America. *Npj Climate and Atmospheric Science*, *6*(1), 141. https://doi.org/10.1038/s41612-023-00461-9

Simpson, I. R., McKinnon, K. A., Kennedy, D., Lawrence, D. M., Lehner, F., & Seager, R. (2024). Observed humidity trends in dry regions contradict climate models. *Proceedings of the National Academy of Sciences*, *121*(1), e2302480120. https://doi.org/10.1073/pnas.2302480120

Stevens, B., Adami, S., Ali, T., Anzt, H., Aslan, Z., Attinger, S., Bäck, J., Baehr, J., Bauer, P., Bernier, N., Bishop, B., Bockelmann, H., Bony, S., Bouchet, V., Brasseur, G., Bresch, D. N., Breyer, S., Brunet, G., Buttigieg, P. L., … Ziemen, F. (2023). *Earth Virtualization Engines (EVE)* [Preprint]. ESSD – Global/Meteorology. https://doi.org/10.5194/essd-2023-376

Swain, D. L., Horton, D. E., Singh, D., & Diffenbaugh, N. S. (2016). Trends in atmospheric patterns conducive to seasonal precipitation and temperature extremes in California. *Science Advances*, *2*(4), e1501344. https://doi.org/10.1126/sciadv.1501344

Teng, H., Leung, R., Branstator, G., Lu, J., & Ding, Q. (2022). Warming Pattern over the Northern Hemisphere Midlatitudes in Boreal Summer 1979–2020. *Journal of Climate*, *35*(11), 3479–3494. https://doi.org/10.1175/JCLI-D-21-0437.1

Thompson, V., Kennedy-Asser, A. T., Vosper, E., Lo, Y. T. E., Huntingford, C., Andrews, O., Collins, M., Hegerl, G. C., & Mitchell, D. (2022). The 2021 western North America heat wave among the most extreme events ever recorded globally. *Science Advances*, *8*(18), eabm6860. https://doi.org/10.1126/sciadv.abm6860

Thompson, V., Mitchell, D., Hegerl, G. C., Collins, M., Leach, N. J., & Slingo, J. M. (2023). The most at-risk regions in the world for high-impact heatwaves. *Nature Communications*, *14*(1), 2152. https://doi.org/10.1038/s41467-023-37554-1

Urdiales-Flores, D., Zittis, G., Hadjinicolaou, P., Osipov, S., Klingmüller, K., Mihalopoulos, N., Kanakidou, M., Economou, T., & Lelieveld, J. (2023). Drivers of accelerated warming in Mediterranean climate-type regions. *Npj Climate and Atmospheric Science*, *6*(1), 97. https://doi.org/10.1038/s41612-023-00423-1

Vautard, R., Cattiaux, J., Happé, T., Singh, J., Bonnet, R., Cassou, C., Coumou, D., D'Andrea, F., Faranda, D., Fischer, E., Ribes, A., Sippel, S., & Yiou, P. (2023). Heat extremes in Western Europe increasing faster than simulated due to atmospheric circulation trends. *Nature Communications*, *14*(1), 6803. https://doi.org/10.1038/s41467-023-42143-3

Wang, P., Yang, Y., Xue, D., Ren, L., Tang, J., Leung, L. R., & Liao, H. (2023). Aerosols overtake greenhouse gases causing a warmer climate and more weather extremes toward carbon neutrality. *Nature Communications*, *14*(1), 7257. https://doi.org/10.1038/s41467-023-42891-2

White, R. H., Anderson, S., Booth, J. F., Braich, G., Draeger, C., Fei, C., Harley, C. D. G., Henderson, S. B., Jakob, M., Lau, C.-A., Mareshet Admasu, L., Narinesingh, V., Rodell, C., Roocroft, E., Weinberger, K. R., & West, G. (2023). The unprecedented Pacific Northwest heatwave of June 2021. *Nature Communications*, *14*(1), 727. https://doi.org/10.1038/s41467-023-36289-3

White, R. H., Kornhuber, K., Martius, O., & Wirth, V. (2022). From Atmospheric Waves to Heatwaves: A Waveguide Perspective for Understanding and Predicting Concurrent, Persistent, and Extreme Extratropical Weather. *Bulletin of the American Meteorological Society*, *103*(3), E923–E935. https://doi.org/10.1175/BAMS-D-21-0170.1

Woollings, T., Barriopedro, D., Methven, J., Son, S.-W., Martius, O., Harvey, B., Sillmann, J., Lupo, A. R., & Seneviratne, S. (2018). Blocking and its Response to Climate Change. *Current Climate Change Reports*, *4*(3), 287–300. https://doi.org/10.1007/s40641-018-0108-z

Yuval, J., & O'Gorman, P. A. (2020). Stable machine-learning parameterization of subgrid processes for climate modeling at a range of resolutions. *Nature Communications*, *11*(1), 3295. https://doi.org/10.1038/s41467-020-17142-3

Zachariah, M., Philip, S., Pinto, I., Vahlberg, M., Singh, R., Otto, F., Barnes, C., & Kimutai, J. (2023). *Extreme heat in North America, Europe and China in July 2023 made much more likely by climate change*. Imperial College London. https://doi.org/10.25561/105549

## Supporting Information for

# Global emergence of regional heatwave hotspots outpaces climate model projections

**K. Kornhuber[1,2,3,4*], S. Bartusek[2,5], R. Seager[2], H. J. Schellnhuber[1*], M. Ting[2,3]**
[1]International Institute for Applied Systems Analysis (IIASA), Laxenburg, Austria
[2]Lamont-Doherty Earth Observatory, Columbia University, New York, NY, United States
[3]Columbia Climate School, Columbia University, New York, NY, United States
[4]Potsdam Institute for Climate Impact Research, Potsdam, Germany
[5]Department of Earth and Environmental Sciences, Columbia University, NY, United States

*Corresponding Authors:
K. Kornhuber: kornhuber@iiasa.ac.at
H. J Schellnhuber: schellnhuber@iiasa.ac.at

**This PDF file includes:**

Figures S1 to S11
Tables S1

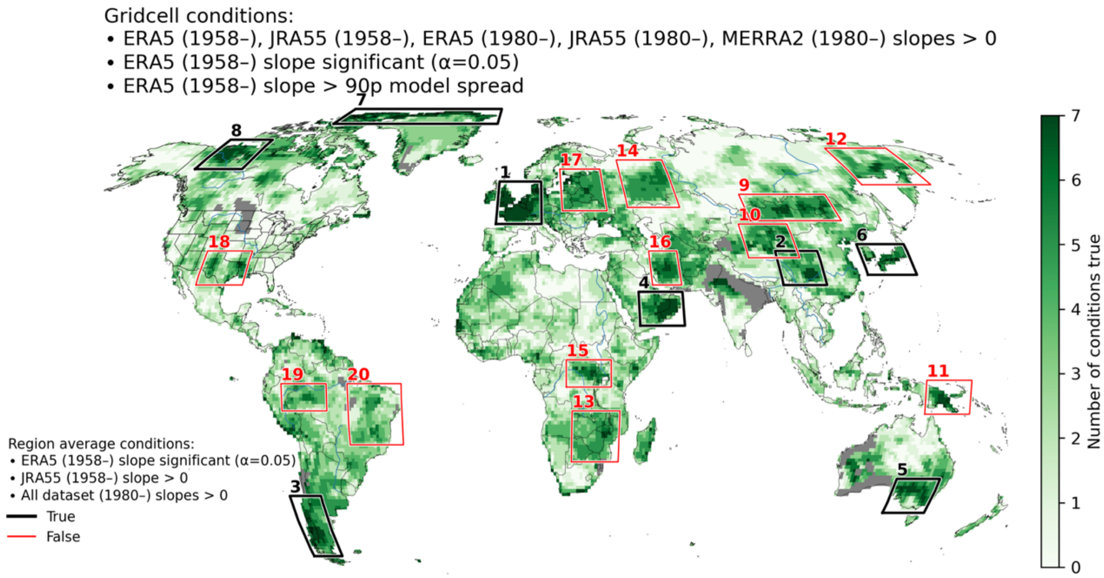


**Figure S1 Global map displaying the robustness of regional tail widening and model biases ranked by seven conditions.** The conditions are as follows: Conditions 1-5 positive trends across reanalysis datasets and time periods (i. ERA5 (1958-2022), ii. JRA55 (1958-2022), iii. ERA5 (1980-2022), iv. JRA55 (1980- 2022), v. MERRA2 (1980 - 2022 ))**,** vi. significant long term trend in ERA5 (1958- 2022, $p < 0.05$), which is also vii. stronger in magnitude than the $90^{th}$ percentile of the model spread (n=49). Regions around areas of interest are outlined above (numbered 1-20). These regions were tested for trends in their regional averages. Regions outlined in black (1,2,3,4,5,6,8), meet the region-average conditions outline on the bottom right, and were therefore selected to be discussed in detail in the main manuscript (Figs. 2, 3, S4). Trends and boxplots for all remaining regions are shown in Fig. S2. and Fig. S3.

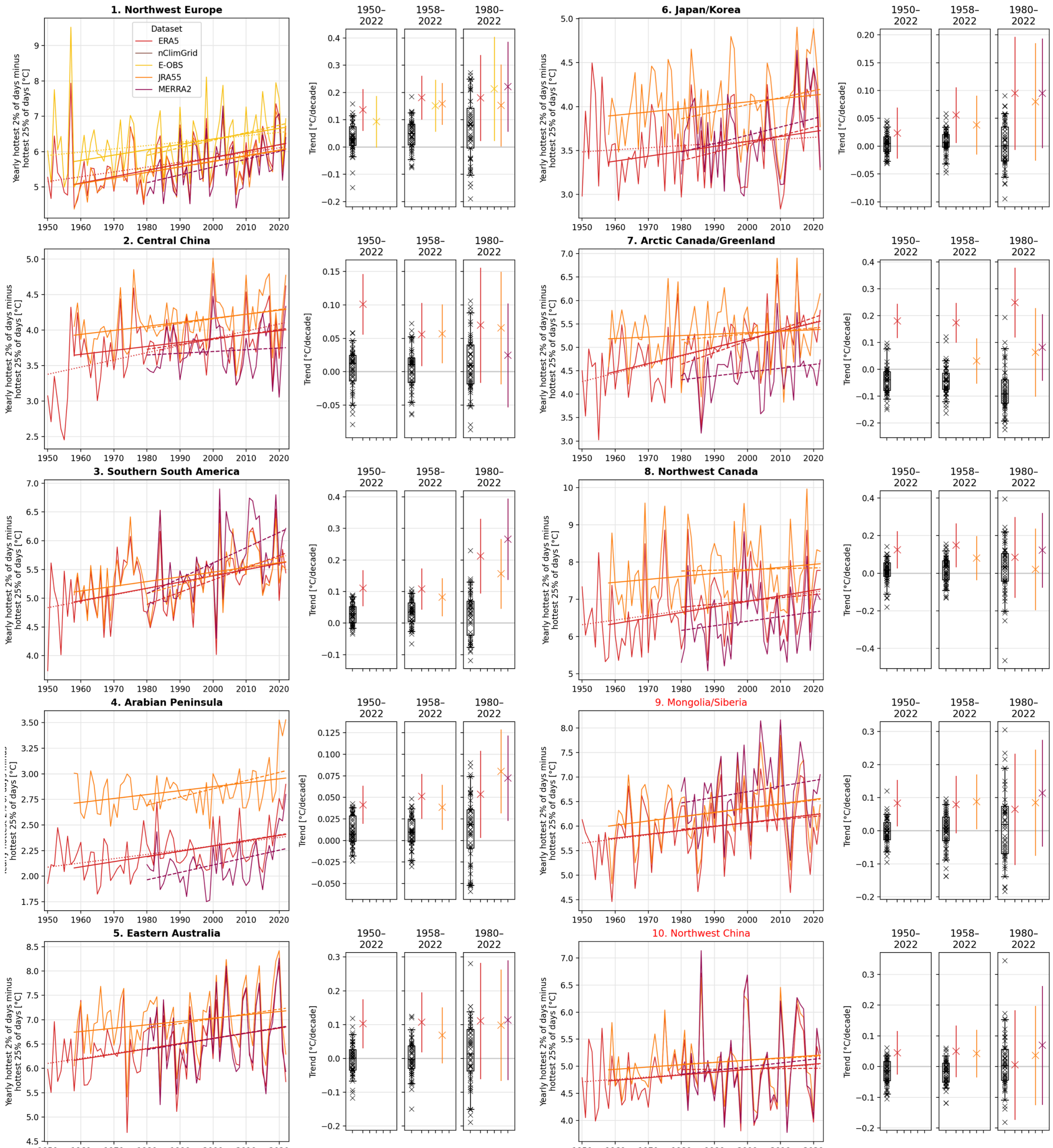


**Figure S2** Regional timeseries in tail widening and a comparison of distributions of modelled changes over three different time-periods and corresponding reanalysis and gridded station observation (E-OBS, nClimGrid) datasets. Definitions of regions 1-10 are shown in Fig. S1. An analysis of regions 11-20 is provided in Fig. S3.

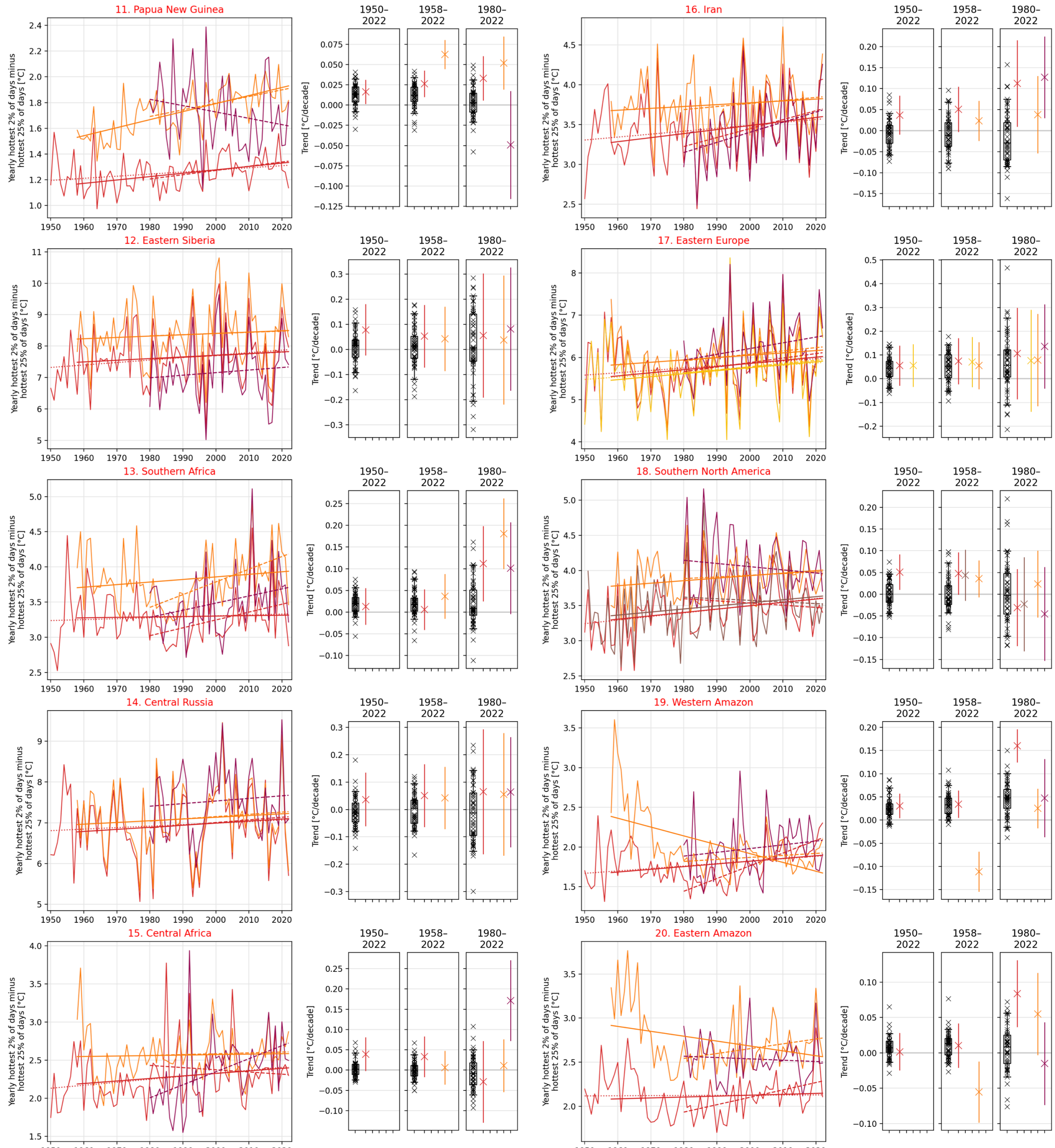


**Figure S3** As in S2 but for regions 11-20. Regional timeseries in tail widening and a comparison of distributions of modelled changes over three different time-periods and corresponding reanalysis and gridded station observation (E-OBS, nClimGrid) datasets. Definitions of regions 11-20 are shown in Fig. S1.

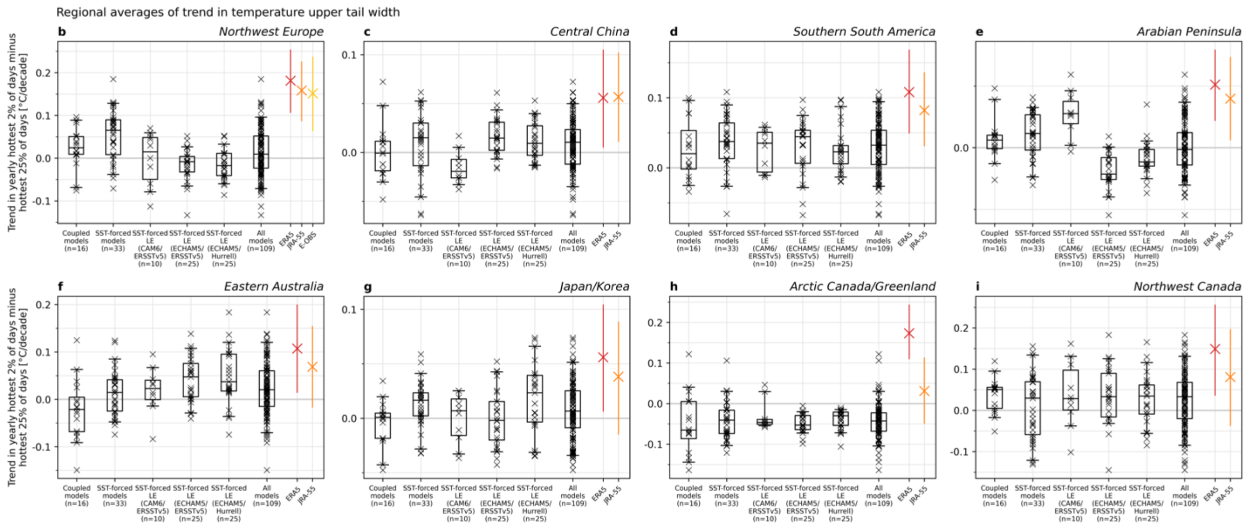


**Figure S4** As in Figure 3b–i but including three SST-forced large ensembles (60 members in total) outside of the 49 HighResMIP project model runs provided in Fig. 3. In each panel, the first two boxplots and the ERA5 (red), JRA-55 (orange), and E-OBS (yellow) datapoints and uncertainty range are exactly as in Figure 3b–i. The third boxplot displays regional trends from a 10-member ensemble of CAM6 forced by ERSSTv5 historical SSTs, covering 1958–2021. The fourth boxplot shows the same from a 25-member ensemble of ECHAM5 forced by ERSSTv5 covering 1958–2020, and the fifth from a 25-member ensemble of ECHAM5 forced by Hurrell SSTs covering 1958–2020. Note that each of the three extra ensembles shown here do not cover the entire time-period 1958–2022 considered in the main analysis. The sixth boxplot aggregates all 109 model realizations. The ECHAM5 runs (Roeckner et al., 2003) were accessed through the NOAA Facility for Weather and Climate Assessments (FACTS) repository (Murray et al., 2020). The CAM6 runs were accessed through the NCAR Climate Data Gateway thanks to the NCAR Climate Variability & Change Working Group (CVCWG).

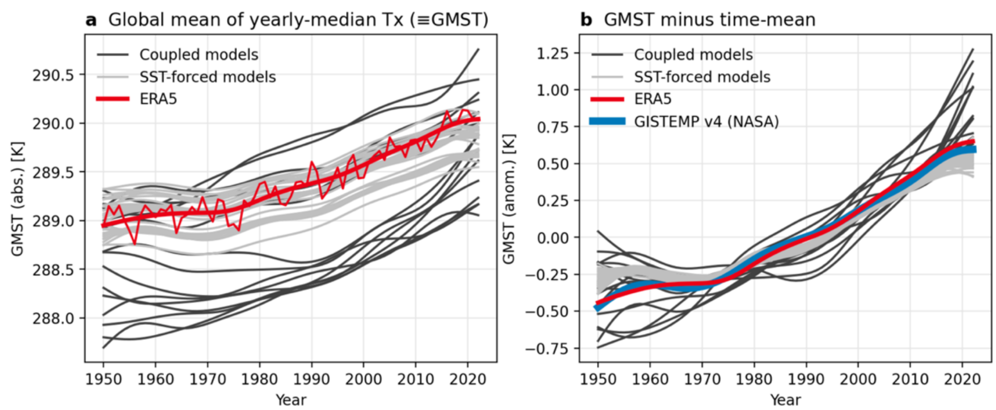


**Figure S5** Demonstration of procedure to calculate smoothed global mean near surface temperature (GMST) time series for each model realization and observations, which are used as a trend covariate instead of time in Figs. S3–S4. In **a**, the thin red line shows the global mean (land and ocean points included) of each grid point's annual median Tx. The thick red line shows this time series smoothed by a low-pass filter to retain only variability of frequencies over 10 years (i.e. a 10-yearly cutoff, third-order Butterworth filter, applied forward and backward). In **b**, this smoothed time series is compared against the widely-used NASA GISTEMP v4 GMST time series, subject to the same smoothing (and with the time-means of each over the whole 1950–2022 period removed). Their high similarity justifies the use of Tx data and annual medians to generate the GMST time series. Light and dark gray lines in **a** and **b** show smoothed GMST time series for model data.

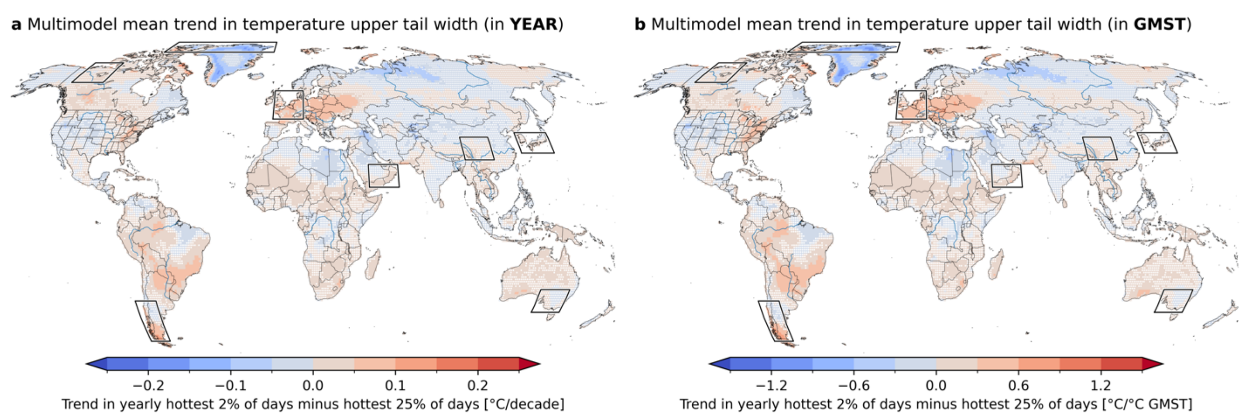


**Figure S6** As in Fig. 2a but **a** multi-model mean trend in the changes in the differences of the hottest 2% of annual maximum of daily maximum temperature (Tx) per year with the average of the 25% of days (annual 87.5$^{th}$ percentile of Tx) percentile of the annual maximum temperature at each grid point for years 1950-2022 (as Fig. 2a but for models) **b** the same variables but scaling local temperatures with global mean temperatures.

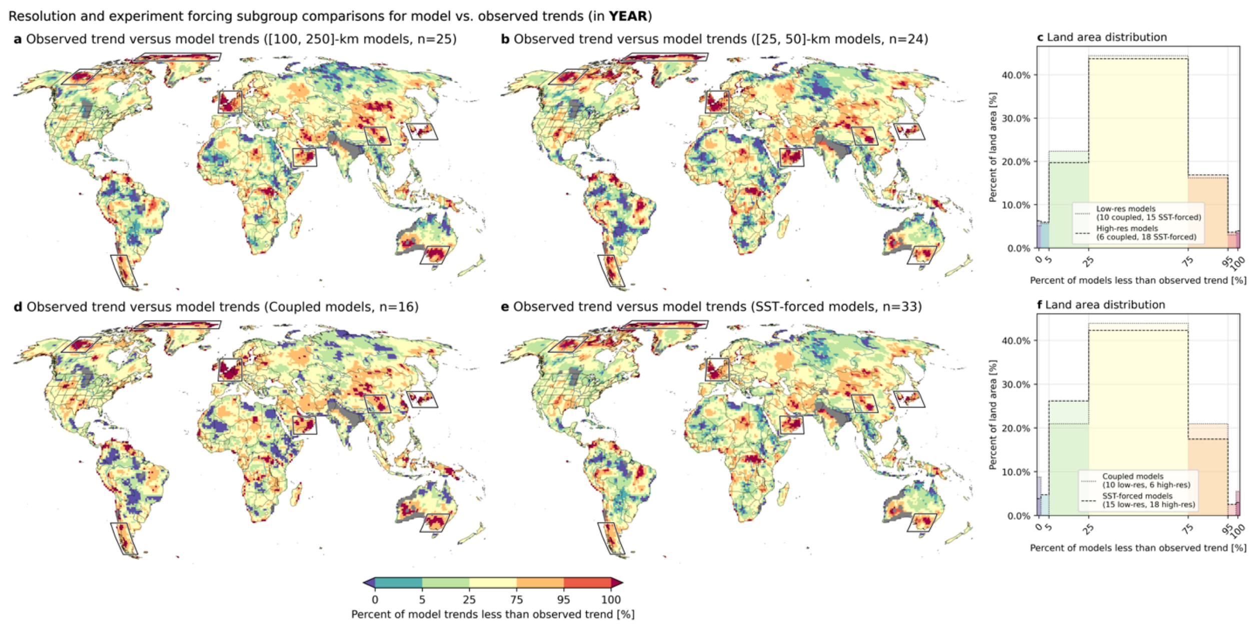


**Figure S7 Observed trends in comparison with the models used and distinguished by their resolution and to atmosphere-ocean coupling frameworks a, b, d, e** Comparison of observed trends (ERA5) in the widening of the upper quartile (see Fig. 3a) in a range of different model subsets and architectures provided **c, f** Collapsing the maps in **a, b, d, e** into histograms. In **c**, histograms provide estimates of the global distribution of the percentages provided in a and b. Color values match the color map provided in the bottom of the figure comparing models with high (n=25) and low resolution (n=24). A high percentage value for the 25$^{th}$ – 75$^{th}$ percentile signifies a better agreement with trends based on reanalysis, while high values in the lower (upper) percentiles relate to an under (over) estimation of trends in models, on a gridcell-by-gridcell basis. The histograms in **f** show the same for trends over land area based on coupled (n-16) vs. SST-forced experiments (n=33). **d** and **e**, respectively.

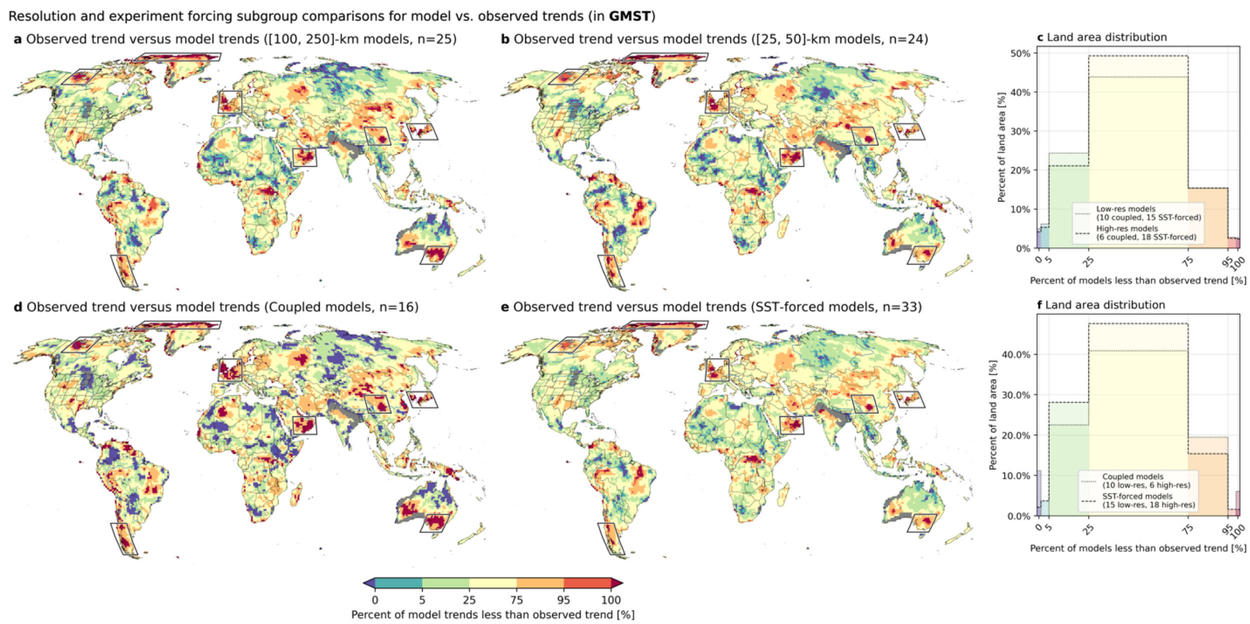


**Figure S8 As in Fig. S7 but for GMST level covariate instead of years. a, b, d, e** Comparison of observed trends (ERA5) in the widening of the upper quartile (see Fig. 3a) in a range of different model subsets and architectures provided **c, f** Collapsing the maps in **a, b, d, e** into histograms. In **c**, histograms provide estimates of the global distribution of the percentages provided in a and b. Color values match the color map provided in the bottom of the figure comparing models with high (n=25) and low resolution (n=24). A high percentage value for the 25$^{th}$ – 75$^{th}$ percentile signifies a better agreement with trends based on reanalysis, while high values in the lower (upper) percentiles relate to an under (over) estimation of trends in models, on a gridcell-by-gridcell basis. The histograms in **f** show the same for trends over land area based on coupled (n-16) vs. SST-forced (n-33) experiments. **d** and **e**, respectively.

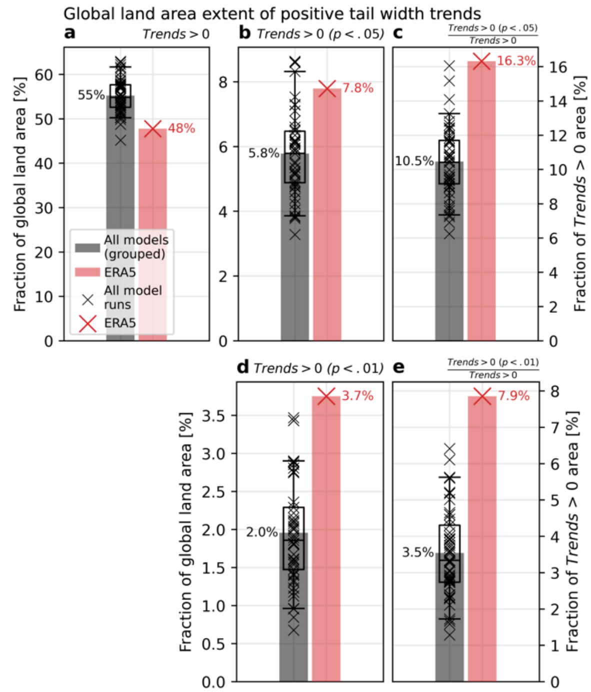


**Figure S9** Comparison of global fraction of land area with **a** positive trends, **b** positive trends which are statistically significant (p < 0.05) and **c** the fraction of positive trends which are also statistically significant (p < 0.05) (right y-axis). **d** Fraction of global land area over which positive trends are significant with a p-value of p < 0.01 and **c** the respective fraction compared to all grid points with positive trends (right y-axis).

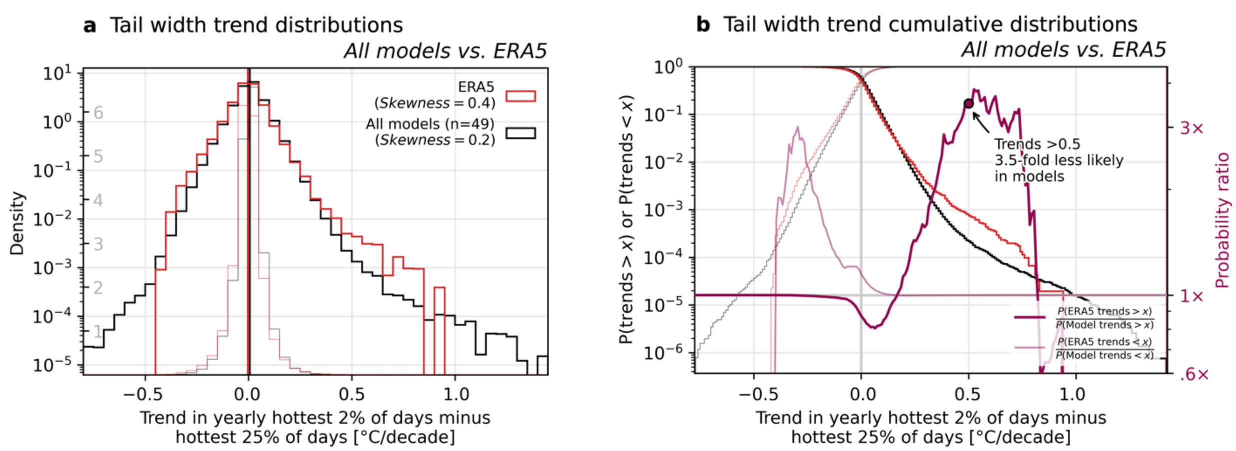


**Fig. S10** Alternative depiction of data shown in Fig. 4 providing a histogram of all models combined in **a** and cumulative density distributions in **b** across positive and negative trends instead of providing values for each side of the distribution separately. Trends that exceed 0.5 0.5 °C/decade irrespective of sign are underestimated by a factor of 3.5.

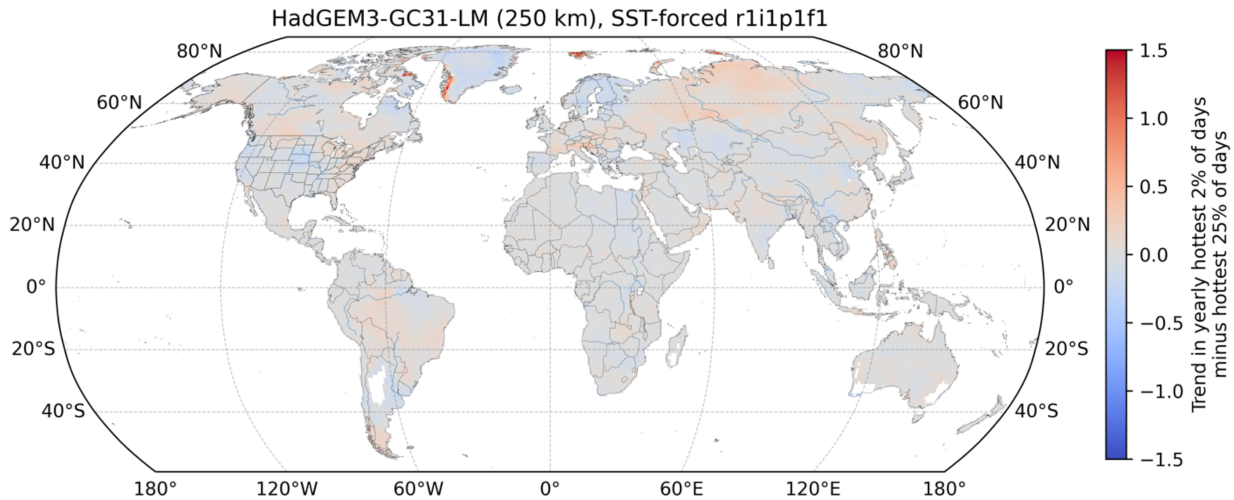


**Figure S11** Modelled trends in the hottest 2% compared to the upper 25% for an ensemble member based on HadGEM3. Strong trends are visible in single grid-points in Arctic regions and might be related to modelled singularities linked to assumptions around land and/or sea ice coverage.

**Table S1:** Model runs and characteristics used in this analysis. Note that some models feature more than one ensemble member.

| Institution | Model | Nominal resolution | Configuration | Number of members |
|---|---|---|---|---|
| AS-RCEC | HiRAM-SIT-HR | 25 km | SST-forced | 1 |
| AS-RCEC | HiRAM-SIT-LR | 50 km | SST-forced | 1 |
| CAS | FGOALS-f3-L | 100 km | SST-forced | 1 |
| CNRM-CERFACS | CNRM-CM6-1 | 250 km | SST-forced | 8 |
| CNRM-CERFACS | CNRM-CM6-1 | 250 km | Coupled | 2 |
| CNRM-CERFACS | CNRM-CM6-1-HR | 50 km | SST-forced | 9 |
| CNRM-CERFACS | CNRM-CM6-1-HR | 50 km | Coupled | 2 |
| EC-Earth-Consortium | EC-Earth3P | 100 km | SST-forced | 1 |
| EC-Earth-Consortium | EC-Earth3P | 100 km | Coupled | 2 |

| | | | | |
|---|---|---|---|---|
| EC-Earth-Consortium | EC-Earth3P-HR | 50 km | SST-forced | 3 |
| EC-Earth-Consortium | EC-Earth3P-HR | 50 km | Coupled | 3 |
| MIROC | NICAM16-7S | 100 km | SST-forced | 1 |
| MIROC | NICAM16-8S | 50 km | SST-forced | 1 |
| MOHC | HadGEM3-GC31-MM | 100 km | SST-forced | 1 |
| MOHC | HadGEM3-GC31-MM | 100 km | Coupled | 2 |
| MOHC | HadGEM3-GC31-LL | 250 km | Coupled | 3 |
| MOHC | HadGEM3-GC31-LM | 250 km | SST-forced | 1 |
| MOHC | HadGEM3-GC31-HM | 50 km | SST-forced | 1 |
| MPI-M | MPI-ESM1-2-HR | 100 km | SST-forced | 1 |
| MPI-M | MPI-ESM1-2-HR | 100 km | Coupled | 1 |
| MPI-M | MPI-ESM1-2-XR | 50 km | Coupled | 1 |
| MRI | MRI-AGCM3-2-H | 25 km | SST-forced | 1 |
| MRI | MRI-AGCM3-2-S | 25 km | SST-forced | 1 |
| NOAA-GFDL | GFDL-CM4C192 | 100 km | SST-forced | 1 |